Pergamon

Int. J. Solids Structures Vol. 32, No. 11, pp. 1555–1570, 1995
Copyright © 1995 Elsevier Science Ltd
Printed in Great Britain. All rights reserved
0020-7683/95 $9.50 + .00

0020-7683(94)00199-5

STRESS STATES AT NEIGHBORING FIBERS INDUCED BY SINGLE-FIBER INTERPHASE DEFECTS

H. S. CHOI and J. D. ACHENBACH
Center for Quality Engineering and Failure Prevention, Northwestern University, Evanston, IL 60208, U.S.A.

(*Received* 19 *November* 1993; *in revised form* 8 *August* 1994)

Abstract—A reduced interphase stiffness of a single fiber (the dissimilar fiber) in a unidirectionally reinforced composite gives rise to stress deviations in its own interphase, as well as in the interphases of neighboring fibers, relative to the stresses in a perfect composite. For transverse loading and an arbitrary cross-sectional distribution of the fibers, a general method is presented to calculate these stress deviations, based on solutions by the boundary element method of boundary integral equations for the dissimilar fiber and neighboring fibers. In this method nearest and next-nearest fibers are taken into account. The interphases are represented by the spring layer model. Detailed numerical results are presented for the special case of a hexagonal array composite. Results are compared for calculations taking into account nearest and next-nearest neighbors. Stresses at the matrix sides of the interphases and energy densities in the interphases have been calculated for the dissimilar fiber and for the next-nearest neighbors. These stresses have also been obtained for the case that the dissimilar fiber has interphase flaws.

INTRODUCTION

The overall mechanical properties and the strength of fiber-reinforced composites are significantly affected by the properties of very thin layers at the fiber–matrix interfaces, i.e. by fiber–matrix interphases. Several authors have investigated the effects of interphase compliance and interphase flaws on the effective elastic constants of the composite material. In these studies interphases have generally been represented by the spring-layer model. In this model the interphases are treated as very thin zones of unspecified thickness. The radial and tangential tractions are continuous across the interphase, but the displacements may be discontinuous between fiber and matrix due to the presence of the interphase. It has generally been assumed that the tractions are proportional to the corresponding displacement discontinuities. The proportionality constants characterize the stiffness of the interphase. This "spring-layer model" has been employed by many authors, e.g. Benveniste (1985), Steif and Hoysan (1987), Hashin (1990) and Achenbach and Zhu (1989). Benveniste (1985) calculated the effective modulus of a composite reinforced by spherical particles which are not well bonded to the matrix. Steif and Hoysan (1987) used an energy method for calculating the longitudinal stiffness of aligned short-fiber composites with imperfectly bonded interfaces. Hashin (1990, 1991) used the spring interphase model in his analysis of the thermoelastic behavior of a fiber reinforced composite as well as that of a particulate composite. He (1992) applied extremum principles of the theory of elasticity to composite bodies to obtain simple bounds for the effective elastic properties of two-phase materials with imperfect interfaces. Jasiuk *et al.* (1992) have investigated the effect of a sliding interface on the elastic properties of composites with randomly distributed circular and spherical rigid inclusions. Recently, Gosz *et al.* (1992) obtained the transverse constitutive response of a hexagonal array composite using a combined analytical and numerical method.

The effect of interphase flaws and radial matrix cracks on the overall mechanical properties has been studied by Achenbach and Zhu (1989, 1990) and Achenbach and Choi (1991). These investigations have been carried out for periodic arrays of the fibers, such as rectangular and hexagonal arrays, and it has been assumed that interface flaws and matrix cracks have the same periodic distribution as the fibers. By virtue of these geometrical

simplifications it was possible to consider a basic cell for detailed calculations of the fields of stress and deformation.

In this paper the more general case is considered of a single fiber which has either a smaller interphase stiffness, or whose interphase contains a defect. All the other fibers have the same interphase properties. The stress deviations in the interphases generated by the presence of the dissimilar fiber are calculated and relevant stresses and deformation energy densities in the interphases of the composite with the dissimilar fiber are compared with the corresponding quantities in the perfect composite. This work generalizes an earlier study by Zhu and Achenbach (1991). The approach used in this paper is applicable for linearly elastic behavior of the fibers and the matrix.

FORMULATION

Figure 1 shows a cross-sectional view of a unidirectionally reinforced fiber-composite in which all fibers are of the same radius a and have the same interphase properties, except one: the dissimilar fiber. This fiber has different interphase stiffness properties including the possibility that all or part of the interphase may have zero stiffness, i.e. the fiber may be completely or partially debonded. It is assumed that at a remote location the composite is subjected to uniform normal stresses $P\sigma_0$ and $Q\sigma_0$ in the x and y directions, respectively. The fibers are labelled by the index "q", where the index "0" is used to identify the dissimilar fiber, and where roughly speaking the larger the value of q, the larger the distance from the dissimilar fiber. The circumference of fiber q is denoted by Γ_q. A large contour Γ_∞ is the boundary of an area of interest of the cross section shown in Fig. 1. Inside Γ_∞ there are $N+1$ fibers. Thus $q = 0, 1, 2, \ldots, N$.

Following earlier papers by Achenbach and Zhu (1989, 1990), a very thin compliant interphase between fibers and matrix is modeled by a distribution of mechanical springs across a representative interface. This model implies that the tractions are continuous, but the displacements may be discontinuous across this interface. For linear behavior in the interphase, the relations between the relevant traction and displacement components may then be written as (at $r = a$)

$$-t_r^{\mathrm{m}} = t_r^{\mathrm{f}} = k_r(u_r^{\mathrm{m}} - u_r^{\mathrm{f}}) \quad \text{if} \quad -t_r^{\mathrm{m}} = t_r^{\mathrm{f}} > 0 \tag{1a}$$

$$-t_r^{\mathrm{m}} = t_r^{\mathrm{f}} \quad \text{and} \quad u_r^{\mathrm{m}} = u_r^{\mathrm{f}} \quad \text{if} \quad -t_r^{\mathrm{m}} = t_r^{\mathrm{f}} \leqslant 0 \tag{1b}$$

$$-t_\theta^{\mathrm{m}} = t_\theta^{\mathrm{f}} = k_\theta(u_\theta^{\mathrm{m}} - u_\theta^{\mathrm{f}}) \tag{1c}$$

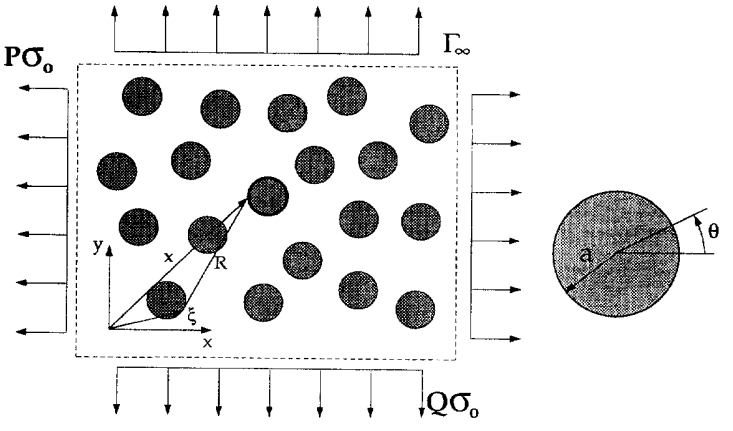

(a) (b)

Fig. 1. (a) Cross-sectional view of the composite with a fiber with dissimilar interphase stiffness, (b) configuration of a fiber.

where t_r and t_θ are the interface tractions in the radial and circumferential directions, respectively. Here and in the sequel, quantities with upper index "m" and "f" are defined in the matrix and the fiber regions, respectively. The addition of eqn (1b) assures that the model will not allow a physically unrealistic radial overlap of the matrix and fiber materials across the interface. The constants k_r and k_θ are proportionality constants which define the mechanical properties of the interphase.

The conditions (1) include the case of perfect bonding ($k_r = k_\theta = \infty$) when the tractions and displacements are continuous and the case of total debonding ($k_r = k_\theta = 0$) when the tractions vanish. In the latter case, it should be noted that the pure sliding condition ($k_r = \infty, k_\theta = 0$) is assumed to exist on the interface when the radial stresses are compressive. If there exist interphase defects like open cracks, say over a region $-\theta_c < \theta < \theta_c < \pi/2$ and $-\theta_c + \pi < \theta < \theta_c + \pi$, then in the domain $0 \leqslant \theta \leqslant \pi/2$ the conditions (1) are valid for $r = a$, $\theta_c < \theta \leqslant \pi/2$, while for $r = a$ and $0 \leqslant \theta \leqslant \theta_c$, we should have interphase crack conditions defined by

$$t_r^m = t_r^f = t_\theta^m = t_\theta^f = 0. \tag{2}$$

It is also noted that for an interphase crack the ligament at the tip of the disbond undergoes a finite stretch when in tension, and consequently the tractions remain bounded. Hence the usual problems of violently oscillating singularities (see Williams, 1959) that are associated with crack-tip fields for a crack in a perfectly bonded interface, do not occur for the spring-layer model. This conclusion follows immediately from eqn (1) and the boundedness of the displacements.

For the generation of interphase cracks, as well as their propagation and arrest, it is feasible to use a critical stress, critical strain, or critical strain energy density criterion, because in the spring-layer model these quantities are well defined near the tip of an interphase crack. In this paper we will employ an energy density criterion, since it combines information on the tensile and shear stresses in the interphase. For the interphase model defined by eqns (1), the strain energy per unit interphase area is easy to calculate. We have

$$U = \frac{(t_r^f)^2}{2k_r} + \frac{(t_\theta^f)^2}{2k_\theta}. \tag{3}$$

It should be noted here that t_r^f is included in U only when t_r^f is positive (tension). It is assumed that compressive values of t_r^f do not affect the integrity of the interphase.

By substituting k into eqn (3) the normalized form of U, $\bar{U} = U\mu^m/(\sigma_0^2 a)$, becomes

$$\bar{U} = \frac{(t_r^f/\sigma_0)^2}{2k_r a/\mu^m} + \frac{(t_\theta^f/\sigma_0)^2}{2k_\theta a/\mu^m} \tag{4}$$

where μ^m is the shear modulus of the matrix material, and σ_0 is the applied stress. It is reasonable to assume that the interphase will break and form an interphase crack in a region of positive radial stress when

$$U \geqslant U^{cr}. \tag{5}$$

When $U = U^{cr}$, the applied stress σ_0 reaches a critical value σ_0^{cr} which can be related to U^{cr} by eqn (4) as

$$\sigma_0^{cr} = \left[\frac{\mu^m}{a}\frac{U^{cr}}{\bar{U}}\right]^{\frac{1}{2}} \tag{6}$$

An analysis of the initiation and propagation of matrix cracks must also be based on an appropriate criterion. For a perfect composite subjected to tensile stresses, numerical

results show, in agreement with physical intuition, see e.g. Achenbach and Zhu (1989, 1990), that the circumferential tensile stress at the fiber–matrix interphase is the largest tensile stress component in the matrix material. As a crack initiation criterion we choose

$$\sigma_\theta \geqslant \sigma^{cr} \tag{7}$$

where σ^{cr} is a critical stress of the matrix material for matrix crack initiation.

The displacement and traction components for the case that no dissimilar fiber is present (perfect composite) are denoted by $u_i^{fp}(x)$ and $t_i^{fp}(x)$ for the fibers, and $u_i^{mp}(x)$ and $t_i^{mp}(x)$ for the matrix material. The deviations of these quantities due to the presence of a dissimilar fiber are denoted by $\bar{u}_i^f(x)$, $\bar{t}_i^f(x)$, $\bar{u}_i^m(x)$ and $\bar{f}_i^m(x)$. The total displacement and traction fields in the presence of a dissimilar fiber may then be written as

$$u_i^f(x) = u_i^{fp}(x) + \bar{u}_i^f(x) \tag{8a}$$

$$u_i^m(x) = u_i^{mp}(x) + \bar{u}_i^m(x) \tag{8b}$$

$$t_i^f(x) = t_i^{fp}(x) + \bar{t}_i^f(x) \tag{8c}$$

$$t_i^m(x) = t_i^{mp}(x) + \bar{t}_i^m(x). \tag{8d}$$

The interface conditions corresponding to the case of a different interface constant are obtained by replacing in eqns (1a), (1b) and (1c) the total tractions t_r^m, t_θ^m, t_r^f, and t_θ^f by the superpositions (8c) and (8d). On the interphase $\Gamma_q (\neq \Gamma_0)$ we then have:

$$-\bar{t}_r^m = k_r(\bar{u}_r^m - \bar{u}_r^f) \tag{9a}$$

$$-\bar{t}_\theta^m = k_\theta(\bar{u}_\theta^m - \bar{u}_\theta^f) \tag{9b}$$

where (r, θ) is a local polar coordinate located at the center of each fiber and Γ_q represents the interfacial boundary of the fiber q. On the interphase Γ_0 we have:

$$-\bar{t}_r^m = -(k_r - \bar{k}_r)(u_r^{mp} - u_r^{fp}) + \bar{k}_r(\bar{u}_r^m - \bar{u}_r^f) \tag{9c}$$

$$-\bar{t}_\theta^m = -(k_\theta - \bar{k}_\theta)(u_\theta^{mp} - u_\theta^{fp}) + \bar{k}_\theta(\bar{u}_\theta^m - \bar{u}_\theta^f). \tag{9d}$$

In eqns (9c) and (9d), $\bar{k}_r$ and $\bar{k}_\theta$ are the interphase constants for the dissimilar fiber.

If the interphase Γ_0 contains an interphase crack in the range of $-\theta_c < \theta < \theta_c < \pi/2$ and $\pi - \theta_c < \theta < \pi + \theta_c$ then eqns (9c and 9d) become

$$-\bar{t}_r^m = -k_r(u_r^{mp} - u_r^{fp}) = t_r^{mp} \tag{9e}$$

$$-\bar{t}_\theta^m = -k_\theta(u_\theta^{mp} - u_\theta^{fp}) = t_\theta^{mp}. \tag{9f}$$

For all interphases Γ_q including Γ_0, the continuity of the tractions across the interphase Γ_q are satisfied by

$$-\bar{t}_r^m = \bar{t}_r^f \tag{10a}$$

$$-\bar{t}_\theta^m = \bar{t}_\theta^f. \tag{10b}$$

By appropriate coordinate transformations the interphase conditions (1a), (1b) and (1c) can be expressed in terms of Cartesian components of tractions and displacements

which will be used in the actual computations. The interphase conditions on the interphase Γ_q ($\neq \Gamma_0$) given by eqns (9a, 9b) may be rewritten as

$$aC_1 \cos\theta \frac{\bar{t}_x^m}{\mu^m} + aC_1 \sin\theta \frac{\bar{t}_y^m}{\mu^m} + \cos\theta(\bar{u}_x^m - \bar{u}_x^f) + \sin\theta(\bar{u}_y^m - \bar{u}_y^f) = 0 \tag{11a}$$

$$-aC_2 \cos\theta \frac{\bar{t}_x^m}{\mu^m} + aC_2 \sin\theta \frac{\bar{t}_y^m}{\mu^m} \sin\theta(\bar{u}_x^m - \bar{u}_x^f) + \cos\theta(\bar{u}_y^m - \bar{u}_y^f) = 0 \tag{11b}$$

where $\bar{t}_{x,y}^m/\mu^m$ has been introduced to enhance the accuracy of the solutions of the simultaneous equations in the numerical calculations using the BEM. The dimensionless compliant constants are defined as

$$C_1 \frac{1}{k_1} = \frac{\mu^m}{ak_r} \quad \text{and} \quad C_2 = \frac{1}{k_2} = \frac{\mu^m}{ak_\theta}. \tag{12a,b}$$

Similarly the interphase conditions (9c, 9d) on the boundary of the dissimilar fiber, Γ_0, can be expressed as

$$a\bar{C}_1 \cos\theta \frac{\bar{t}_x^m}{\mu^m} + a\bar{C}_1 \sin\theta \frac{\bar{t}_y^m}{\mu^m} + \cos\theta(\bar{u}_x^m - \bar{u}_x^f) + \sin\theta(\bar{u}_y^m - \bar{u}_y^f) + a(\bar{C}_1 - C_1)\left(\cos\theta \frac{t_x^{mp}}{\mu^m} + \sin\theta \frac{t_y^{mp}}{\mu^m}\right) = 0 \tag{13a}$$

$$-a\bar{C}_2 \sin\theta \frac{\bar{t}_x^m}{\mu^m} + a\bar{C}_2 \cos\theta \frac{\bar{t}_y^m}{\mu^m} - \sin\theta(\bar{u}_x^m - \bar{u}_x^f) + \cos\theta(\bar{u}_y^m - \bar{u}_y^f) - a(\bar{C}_2 - C_2)\left(\sin\theta \frac{t_x^{mp}}{\mu^m} - \cos\theta \frac{t_y^{mp}}{\mu^m}\right) = 0 \tag{13b}$$

where

$$\bar{C}_1 = \frac{1}{\bar{k}_1} = \frac{\mu^m}{a\bar{k}_r} \quad \text{and} \quad \bar{C}_2 = \frac{1}{\bar{k}_2} = \frac{\mu^m}{a\bar{k}_\theta}. \tag{14a,b}$$

If the interphase of Γ_0 contains an interphase crack in the range of $-\theta_c < \theta < \theta_c < \pi/2$ and $\pi - \theta_c < \theta < \pi + \theta_c$ then eqns (13a, 13b) become

$$t_x^{mp} = -\bar{t}_x^m \quad \text{and} \quad t_y^{mp} = -\bar{t}_y^m. \tag{15a,b}$$

If the dissimilar interphase Γ_0 has compressive radial tractions over one or more elements on Γ_0 then to prevent the interphase from overlapping, the eqns (13a, 13b) become

$$\bar{u}_x^m = \bar{u}_x^f \quad \text{and} \quad \bar{u}_y^m = \bar{u}_y^f \quad \text{on} \quad \Gamma_0 \quad \text{if } t_r^f < 0. \tag{16a,b}$$

Continuity of tractions across the interphase Γ_q including Γ_0 is satisfied as

$$\bar{t}_x^m = -\bar{t}_x^f \quad \text{and} \quad \bar{t}_y^m = -\bar{t}_y^f \tag{17a,b}$$

BIEs for unidirectional composite with one dissimilar fiber

In earlier papers, see e.g. Achenbach and Zhu (1989, 1990), a boundary integral equation has been derived for the displacements and tractions on the circumference of a fiber inside a basic cell of the composite. Here we write the analogous boundary integral equation for fiber q.

$$\tfrac{1}{2}u_i^{\mathrm{m}}(\xi) = \int_{\Gamma+\Gamma_\infty} U_{ij}^{\mathrm{m}}(x,\xi)t_j^{\mathrm{m}}(x)\,\mathrm{d}\Gamma(x) - \int_{\Gamma+\Gamma_\infty} T_{ij}^{\mathrm{m}}(x,\xi)u_j^{\mathrm{m}}(x)\,\mathrm{d}\Gamma(x), \quad x\in\Gamma,\ \xi\in\Gamma_q \tag{18a}$$

where

$$\Gamma = \sum_{q=0}^{N}\Gamma_q \tag{18b}$$

and

$$U_{ij}^{\mathrm{m}}(x,\xi) = \frac{1}{8\pi\mu^{\mathrm{m}}(1-\nu^{\mathrm{m}})}\left[(3-4\nu^{\mathrm{m}})\ln\left(\frac{1}{R}\right)\delta_{ij} + \frac{\partial R}{\partial_{x_i}}\frac{\partial R}{\partial_{x_j}}\right] \tag{19a}$$

$$T_{ij}^{\mathrm{m}}(x,\xi) = -\left[\lambda^{\mathrm{m}}\frac{\partial}{\partial x_l}U_{il}^{\mathrm{m}}(x,\xi)\delta_{jk} + \mu^{\mathrm{m}}\frac{\partial}{\partial x_k}U_{ij}^{\mathrm{m}}(x,\xi) + \mu^{\mathrm{m}}\frac{\partial}{\partial x_j}U_{ik}^{\mathrm{m}}(x,\xi)\right]n_k(x). \tag{19b}$$

A similar BIE for the solution $u_i^{\mathrm{mp}}(\xi)$ in the matrix of the perfect composite can be written as

$$\tfrac{1}{2}u_i^{\mathrm{mp}}(\xi) = \int_{\Gamma+\Gamma_\infty} U_{ij}^{\mathrm{m}}(x,\xi)t_j^{\mathrm{mp}}(x)\,\mathrm{d}\Gamma(x) - \int_{\Gamma+\Gamma_\infty} T_{ij}^{\mathrm{m}}(x,\xi)u_j^{\mathrm{mp}}(x)\,\mathrm{d}\Gamma(x), \quad x\in\Gamma,\ \xi\in\Gamma_q. \tag{20}$$

Subtracting eqn (20) from eqn (18) gives a BIE for $\bar{u}_i^{\mathrm{m}}(\xi)$ as

$$\begin{aligned}\tfrac{1}{2}\bar{u}_i^{\mathrm{m}}(\xi) = {} & \int_{\Gamma} U_{ij}^{\mathrm{m}}(x,\xi)\bar{t}_j^{\mathrm{m}}(x)\,\mathrm{d}\Gamma(x) - \int_{\Gamma} T_{ij}^{\mathrm{m}}(x,\xi)\bar{u}_j^{\mathrm{m}}(x)\,\mathrm{d}\Gamma(x) \\ & + \int_{\Gamma_\infty} U_{ij}^{\mathrm{m}}(x,\xi)\bar{t}_j^{\mathrm{m}}(x)\,\mathrm{d}\Gamma(x) - \int_{\Gamma_\infty} T_{ij}^{\mathrm{m}}(x,\xi)\bar{u}_j^{\mathrm{m}}(x)\,\mathrm{d}\Gamma(x), \quad x\in\Gamma,\ \xi\in\Gamma_q.\end{aligned} \tag{21}$$

Since the tractions $\bar{t}_i^{\mathrm{m}}(x)$ corresponding to $\bar{u}_i^{\mathrm{m}}(x)$ are self-equilibrating with respect to the center of fiber zero, it follows from Saint-Venant's principle that $\bar{u}_i^{\mathrm{f}}(x)$, $\bar{u}_i^{\mathrm{m}}(x)$, $\bar{t}_i^{\mathrm{f}}(x)$ and $\bar{t}_i^{\mathrm{m}}(x)$ decrease as the field point x moves away from the center of the dissimilar fiber. Hence, the contour can be appropriately chosen so far from the origin that the integrals over the contour Γ_∞ in eqn (21) come to vanish. As an additional approximation it may be assumed that only a small number of neighboring fibers need be included in Γ.

The corresponding BIE for the fiber q may be written as

$$\tfrac{1}{2}u_i^{\mathrm{f}}(\xi) = \int_{\Gamma_q} U_{ij}^{\mathrm{f}}(x,\xi)t_j^{\mathrm{f}}(x)\,\mathrm{d}\Gamma(x) - \int_{\Gamma_q} T_{ij}^{\mathrm{f}}(x,\xi)u_j^{\mathrm{f}}(x)\,\mathrm{d}\Gamma(x), \quad x,\xi\in\Gamma_q. \tag{22}$$

Similarly, substituting eqn (8a) into eqn (22) yields

$$\tfrac{1}{2}\bar{u}_i^{\mathrm{f}}(\xi) = \int_{\Gamma_q} U_{ij}^{\mathrm{f}}(x,\xi)\bar{t}_j^{\mathrm{f}}(x)\,\mathrm{d}\Gamma(x) - \int_{\Gamma_q} T_{ij}^{\mathrm{f}}(x,\xi)\bar{u}_j^{\mathrm{f}}(x)\,\mathrm{d}\Gamma(x)$$

$$-\tfrac{1}{2}u_i^{\mathrm{fp}}(\xi) + \int_{\Gamma_q} U_{ij}^{\mathrm{f}}(x,\xi)t_j^{\mathrm{fp}}(x)\,\mathrm{d}\Gamma(x) - \int_{\Gamma_q} T_{ij}^{\mathrm{f}}(x,\xi)u_j^{\mathrm{fp}}(x)\,\mathrm{d}\Gamma(x), \quad x,\xi\in\Gamma_q. \tag{23}$$

But we know that the terms in the second line of eqn (23) vanish for all fibers in the composite without a dissimilar fiber, so we have

$$\tfrac{1}{2}\bar{u}_i^{\mathrm{f}}(\xi) = \int_{\Gamma_q} U_{ij}^{\mathrm{f}}(x,\xi)\bar{t}_j^{\mathrm{f}}(x)\,\mathrm{d}\Gamma(x) - \int_{\Gamma_q} T_{ij}^{\mathrm{f}}(x,\xi)\bar{u}_j^{\mathrm{f}}(x)\,\mathrm{d}\Gamma(x), \quad x,\xi\in\Gamma_q. \tag{24}$$

For plane strain the circumferential stress $\sigma_\theta^{\mathrm{m}}$ along the matrix side of the interphase may be calculated by

$$\sigma_\theta^{\mathrm{m}} = -\frac{\nu^{\mathrm{m}}}{1-\nu^{\mathrm{m}}}t_r^{\mathrm{m}} + \frac{2\mu^{\mathrm{m}}}{a(1-\nu^{\mathrm{m}})}\left(u_r^{\mathrm{m}} + \frac{\partial u_\theta^{\mathrm{m}}}{\partial\theta}\right) \tag{25}$$

where $\partial u_\theta^{\mathrm{m}}/\partial\theta$ will be obtained by a numerical differentiation method.

Example: *hexagonal-array composite*

Equations (1)–(25) are valid for any distribution of the fibers over the cross section. We will now, however, consider the special case of a hexagonal-array composite as shown in Fig. 2. For the case without a dissimilar fiber the interphase fields have been analysed by Achenbach and Zhu (1989, 1990).

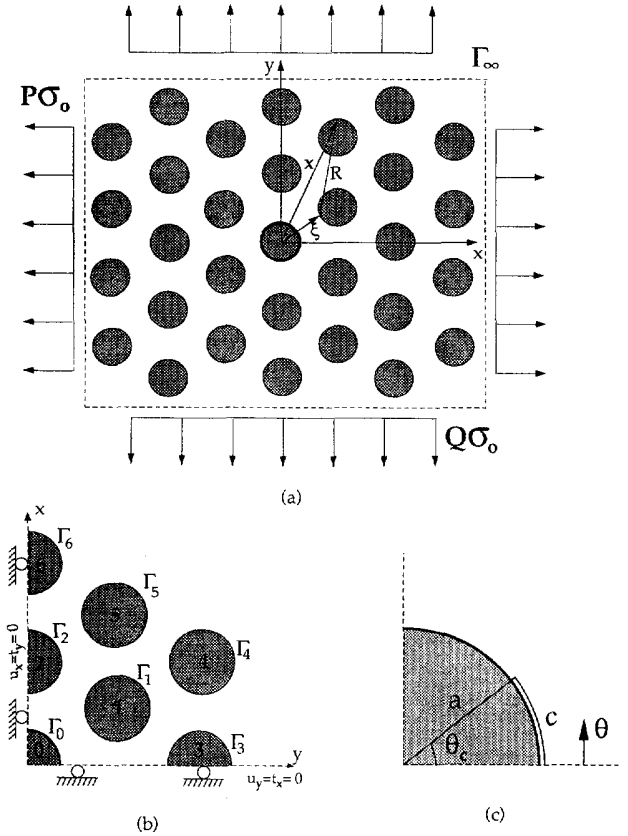

Fig. 2. Configuration for the hexagonal array: (a) the dissimilar fiber 0 has lower interphase stiffness. All other fibers have the same interphase stiffnesses, (b) shows the domain for numerical calculations, and (c) the dissimilar fiber 0 has interphase debonding.

The centers of the regular fibers are located at the following points

$$(x, y) = \left(\frac{\sqrt{3}}{2} bi, \frac{1}{2} bj\right) \quad |i|, |j| = 0, 1, 2, 3, \ldots \quad \text{and} \quad i+j = \text{even integer} \tag{26}$$

where b is the distance between the centers of two adjacent fibers, and $|i|+|j| \neq 0$. A Cartesian coordinate system (x, y) has its origin at the center of the dissimilar fiber.

Because of symmetry with respect to the x- and y-axes we only need to consider the fibers in the first quadrant, as shown in Fig. 2. The nearest neighbors to the dissimilar fiber are denoted fibers 1 and 2, and the next nearest fibers are 3, 4, 5 and 6.

The symmetry conditions on the sides of the first quadrant make it possible to limit the boundary element calculations to that quadrant only. The fundamental solutions which satisfy the symmetry conditions $u_x = t_y = 0$ at $x = 0$ and $u_y = t_x = 0$ at $y = 0$ can be constructed from the full-space fundamental solutions given by eqns (19a)–(19b). For a load applied at (x, y) the construction is easily achieved by placing corresponding loads at the image points of (x, y) in the other three quadrants, as shown in Fig. 3. In terms of $U_{ij}(\boldsymbol{x}, \boldsymbol{\xi})$ and $T_{ij}(\boldsymbol{x}, \boldsymbol{\xi})$ given by eqns (19a)–(19b) (superscript "m" can be disregarded), the first quadrant fundamental solutions $U_{ij}^{Q}(\boldsymbol{x}, \boldsymbol{\xi})$ and $T_{ij}^{Q}(\boldsymbol{x}, \boldsymbol{\xi})$ may be written as

$$U_{ij}^{Q}(\boldsymbol{x}, \boldsymbol{\xi}) = U_{ij}(\boldsymbol{x}, \boldsymbol{\xi}) + \alpha U_{ij}(\boldsymbol{x}, -\bar{\boldsymbol{\xi}}) + \beta U_{ij}(\boldsymbol{x}, -\boldsymbol{\xi}) + \gamma U_{ij}(\boldsymbol{x}, \bar{\boldsymbol{\xi}}), \quad \boldsymbol{x}, \boldsymbol{\xi} \in \text{1st Quadrant} \tag{27a}$$

$$T_{ij}^{Q}(\boldsymbol{x}, \boldsymbol{\xi}) = T_{ij}(\boldsymbol{x}, \boldsymbol{\xi}) + \alpha T_{ij}(\boldsymbol{x}, -\bar{\boldsymbol{\xi}}) + \beta T_{ij}(\boldsymbol{x}, -\boldsymbol{\xi}) + \gamma T_{ij}(\boldsymbol{x}, \bar{\boldsymbol{\xi}}), \quad \boldsymbol{x}, \boldsymbol{\xi} \in \text{1st Quadrant} \tag{27b}$$

where the coefficients α, β and γ take values, $\alpha = \beta = -\gamma = -1$ for $i = 1$ and $-\alpha = \beta = \gamma = -1$ for $i = 2$ and $\bar{\boldsymbol{\xi}}$ denotes the conjugate point of $\boldsymbol{\xi}$.

More detailed expressions for $U_{ij}^{Q}(\boldsymbol{x}, \boldsymbol{\xi})$ and $T_{ij}^{Q}(\boldsymbol{x}, \boldsymbol{\xi})$ are given in the Appendix.

Boundary element method

Equations (18)–(24) have been solved numerically by an application of the boundary element method. The equations have been solved in the first quadrant shown in Figure 2(b) by using the fundamental solutions given by eqns (27a) and (27b). It has been assumed that the deviations in the fields of stress and deformation generated by the interphase properties of the dissimilar fiber 0 extend to the next nearest two fiber-layers only, i.e. to the fibers 1 and 2 in the first fiber-layer and to the fibers 3–6 in the second fiber-layer.

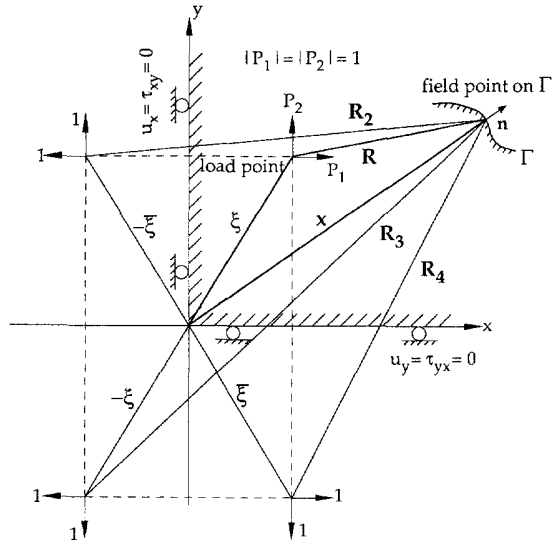

Fig. 3. Geometrical construction of the first quadrant fundamental solutions; $\boldsymbol{\xi} = (\xi_1, \xi_2)$ and $\bar{\boldsymbol{\xi}} = (\xi_1, -\xi_2)$.

The contours, Γ_0, Γ_1, Γ_2, Γ_3, Γ_4, Γ_5 and Γ_6, contain unknown deviations of the tractions and displacements. Along these contours, the integration is performed clockwise for the matrix side integration and counterclockwise for the fiber side. Suppose that the contours Γ_0, Γ_1, Γ_2, Γ_3, Γ_4, Γ_5 and Γ_6 are divided into N_0, N_1, N_2, N_3, N_4, N_5 and N_6 elements, respectively, where the fields are taken as constants over each element. We then have $8N_0$, $8N_1$, $8N_2$, $8N_3$, $8N_4$, $8N_5$ and $8N_6$ unknowns for the integrations over the contours Γ_0, Γ_1, Γ_2, Γ_3, Γ_4, Γ_5 and Γ_6, respectively (two traction and two displacement components on each side of a contour). Consequently we have a total of $8(N_0+N_1+N_2+N_3+N_4+N_5+N_6)$ unknowns. The same number of equations is needed. Equations (21) and (24) give $4(N_0+N_1+N_2+N_3+N_4+N_5+N_6)$ equations and the continuity of tractions, eqn (9), together with eqn (13) on the interface yields $4(N_0+N_1+N_2+N_3+N_4+N_5+N_6)$ equations. Hence the total number of equations is the same as the total number of unknowns. Thus the discretized system of eqns (21) and (24) can be solved numerically. When there are no interphase flaws, all interphases are equally divided, specifically in 120 or 60 elements, such that $4N_0 = N_1 = 2N_2 = 120$ and $2N_3 = N_4 = N_5 = 2N_6 = 60$. When Γ_0 contains a crack, the crack tip element and the element ahead of the crack tip element are further divided into smaller elements to give more accurate results. The number of elements near the crack tip is increased until a further increase does not change the numerical results. Numerical calculations have been carried out for FP/Al composites (see Takahashi and Chou, 1988) with the following properties:

$$\text{Aluminum matrix}: \mu^{\mathrm{m}} = 25.61\ \text{GPa},\ \nu^{\mathrm{m}} = 0.345$$

$$\text{FP}(Al_2O_3)\ \text{fibers}: \mu^{\mathrm{f}} = 157.9\ \text{GPa},\ \nu^{\mathrm{f}} = 0.2.$$

The perfect and the dissimilar interphase constants (k_r, k_θ) and $(\bar{k}_r, \bar{k}_\theta)$ were rendered dimensionless by division by μ^{m}/a, where a is the radius of the fibers. In the computations, the two interphase constants were taken equal in magnitude, and thus $k_r/(\mu^{\mathrm{m}}/a) = k_\theta/(\mu^{\mathrm{m}}/a) = k$. Similarly in the dissimilar interphase $\bar{k}_r/(\mu^{\mathrm{m}}/a) = \bar{k}_\theta/(\mu^{\mathrm{m}}/a) = \bar{k}$.

In the initial state of the calculation the radial interface stress σ_r^{m} $(= \sigma_r^{\mathrm{f}} = t_r^{\mathrm{f}} = -t_r^{\mathrm{m}})$ is computed under the assumption that eqn (1a) applies along the interface of the dissimilar fiber. If a negative radial stress value is obtained over one or more elements and the displacements display an overlap, eqn (1a) is replaced by eqn (1b) and the calculation is redone until the overlap disappears and all boundary conditions are satisfied. Values of $\bar{k} = 0.001, 0.1, 1, 10, 100$ and ∞ were considered for the interphase stiffness of the dissimilar fiber and $k = \infty$ for the neighboring fibers. The fiber volume ratio V_{f} was chosen as 0.2, 0.4, 0.6 or 0.8.

RESULTS

The approximation of including only the nearest and next-nearest neighbors in the BEM calculations would seem to be a reasonable one. The question does, however, arise whether sufficiently accurate results can be obtained by including only the nearest neighbors, i.e. fibers 1 and 2 in Fig. 2. Intuitively it is expected that this simpler approximation will be valid for smaller volume densities, V_{f}, of the fibers. Test calculations have been carried out for the case of uniaxial tension, for $V_{\mathrm{f}} = 0.2$ and $V_{\mathrm{f}} = 0.8$, and $\bar{k} = 10$ and $\bar{k} = 1$. The results are shown in Fig. 4. It is noted that the inclusion of the next-nearest neighboring fibers (solid lines) makes a small difference which becomes somewhat more pronounced for smaller values of $\bar{k}$ and larger values of V_{f}. The numerical results presented in the sequel have been carried out taking into account only the next nearest neighbors.

Figure 5 shows the stress fields σ_r/σ_0, $\sigma_{r\theta}/\sigma_0$, σ_θ/σ_0 at the matrix side of the interphase and the normalized strain energy density $\bar{U}$ in the interphase of the dissimilar fiber for the case of tension in the x direction. The radial stress in the region of tensile stresses decreases as the interphase stiffness, $\bar{k}$, of the dissimilar fiber decreases. The maximum value of the hoop stress, near $\theta = 75°$, does, however, increase as $\bar{k}$ decreases. Other calculations not

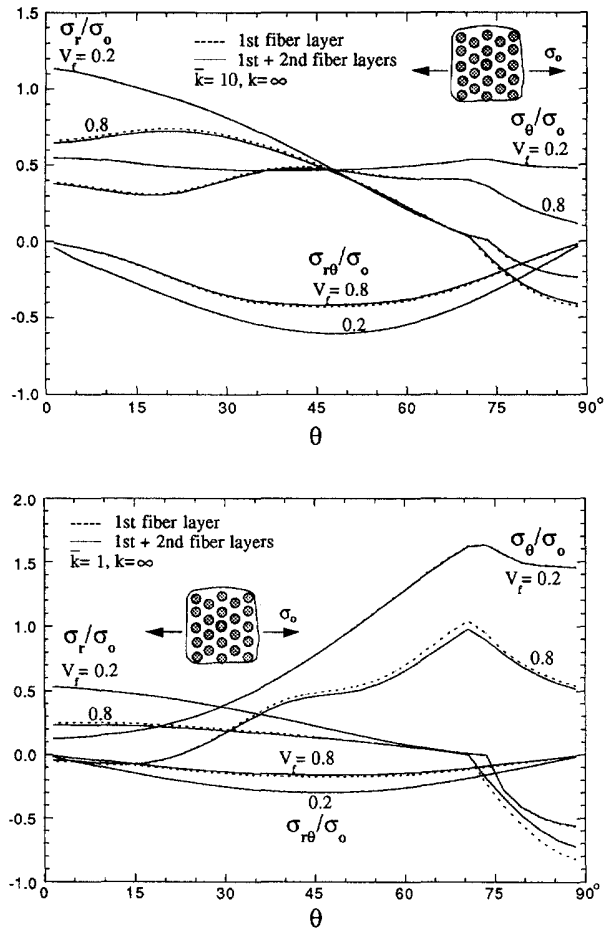

Fig. 4. Comparison of stress fields in the interphase of the dissimilar fiber obtained by considering only the first fiber layer (dashed lines) and considering both the first and second fiber layers (solid lines) for the selected values of V_f and $\bar{k}$.

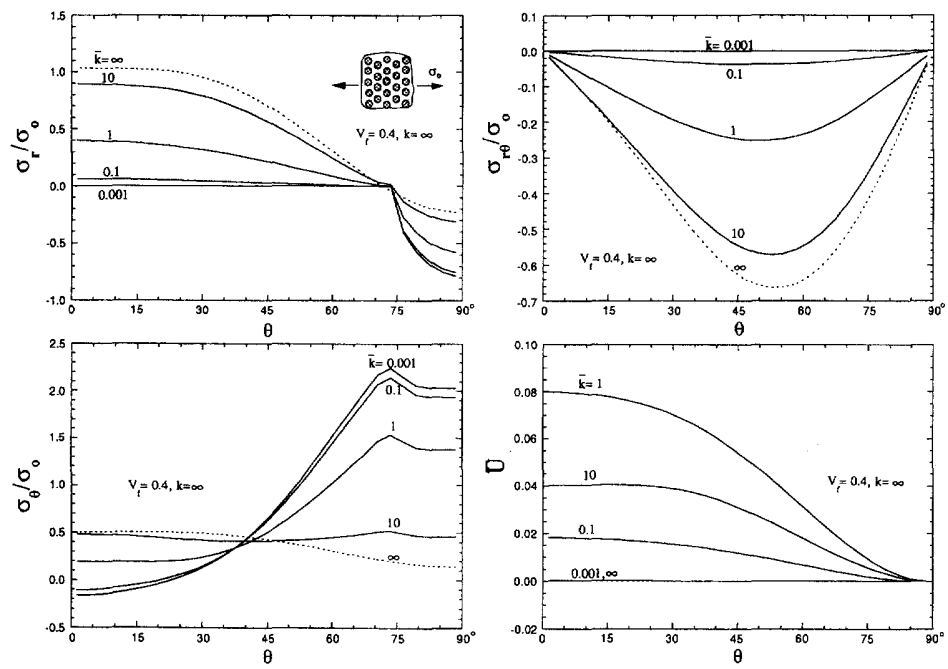

Fig. 5. σ_r/σ_0, $\sigma_{r\theta}/\sigma_0$, σ_θ/σ_0 at the matrix side of the interphase and $\bar{U}$ in the interphase of the dissimilar fiber 0, for various $\bar{k}$ with $k = \infty$ and $V_f = 0.4$, and for uniaxial tension in the x direction.

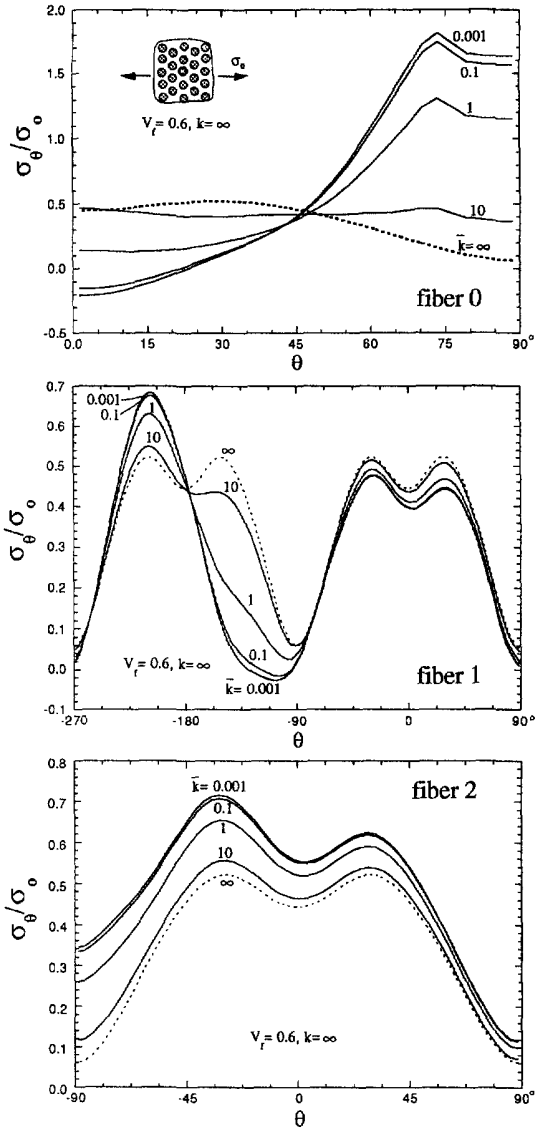

Fig. 6. σ_θ/σ_0 at the matrix side of the interphases of the dissimilar fiber 0 and the neighboring fibers 1 and 2, for various $\bar{k}$ with $k = \infty$ and $V_f = 0.6$, and for uniaxial tension in the x direction.

reported here show that the magnitudes of σ_r/σ_0, $\sigma_{r\theta}/\sigma_0$, σ_θ/σ_0 and $\bar{U}$ at the dissimilar interphase are slightly less than those of σ_r/σ_0, $\sigma_{r\theta}/\sigma_0$, σ_θ/σ_0 and $\bar{U}$ at the interphases of the perfect composite with the same interphase stiffness ($k = \bar{k}$) in all interphases. That difference becomes larger for lower interphase stiffness $\bar{k}$.

Figure 6 shows the hoop stresses along the matrix-side of the interphases of the three fibers 0, 1 and 2 with $V_f = 0.6$ for various $\bar{k}$: $\bar{k} = \infty$, 10, 1, 0.1, 0.001. Comparison with the results of Fig. 5 shows that the hoop stress σ_θ/σ_0 of the dissimilar fiber for $V_f = 0.6$ is slightly smaller than that for $V_f = 0.4$. The hoop stresses of the neighboring fibers 1 and 2 slightly increase as $\bar{k}$ decreases. The result shows that for low $\bar{k}$ the positive maximum hoop stress $(\sigma_\theta)_{max}$ occurs near $\theta = 70°$ for the dissimilar fiber, near $\theta = -208°$ for the neighboring fiber 1 and near $\theta = -30°$ for fiber 2.

Figure 7 shows the hoop stresses along the matrix side of the interphase of the dissimilar fiber and the strain energy in the interphase for the case of uniaxial compression in the x direction. When the composite is compressed in the x direction the maximum tensile hoop stress occurs at $\theta = 0°$ for low $\bar{k}$ and at $\theta = 90°$ for high $\bar{k}$ (above 10). For the dissimilar

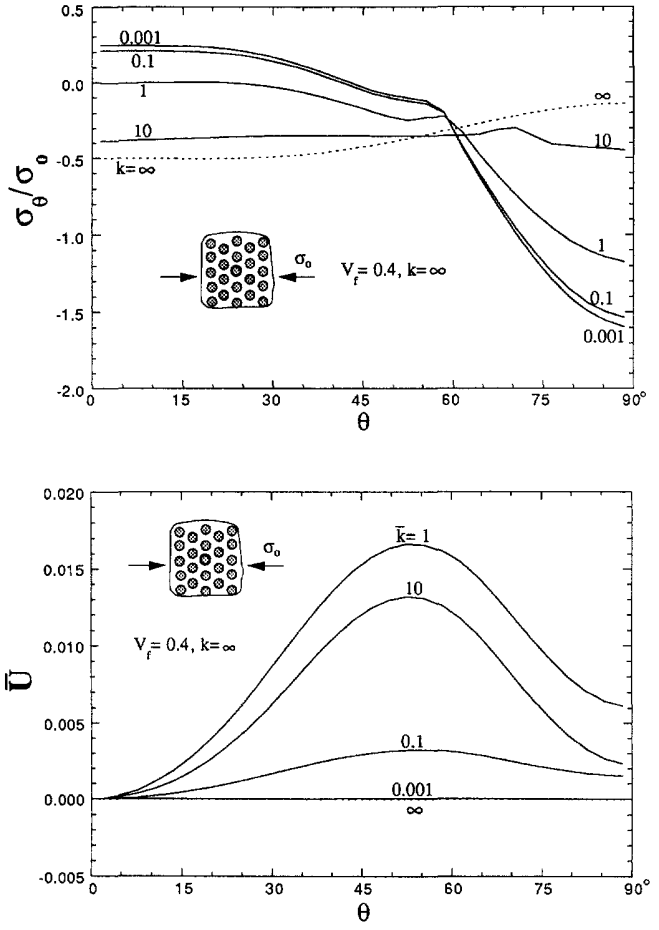

Fig. 7. σ_θ/σ_0 at the matrix side of the interphase and $\bar{U}$ in the interphase of the dissimilar fiber 0, for various $\bar{k}$ with $k = \infty$ and $V_f = 0.4$, for uniaxial compression in the x direction.

fiber the maximum strain energy U_{max} occurs near $\theta = 55°$ for $\bar{k} = 1$. The hoop stresses of the neighboring fibers 1 and 2 are compressive for any $\bar{k}$.

When the interphase of the dissimilar fiber contains interphase cracks as shown in Fig. 2(c), the behavior of σ_r/σ_0, $\sigma_{r\theta}/\sigma_0$, σ_θ/σ_0 and $\bar{U}$ depends greatly upon the interphase stiffness $\bar{k}$. Figure 8 shows σ_θ/σ_0 and $\bar{U}$ for various $\bar{k}$ along the matrix side of the interphase of the dissimilar fiber for an interphase crack of length $\bar{c} = c/0.05236a = 9$, for the case of an uniaxial tensile stress σ_0 in the x direction. The maximum hoop stress and energy density are obtained at the crack tip. The magnitude of the hoop stress increases with increasing values of $\bar{k}$. The results for σ_θ/σ_0 at the neighboring fibers 1 and 2 are also shown in Fig. 8. The overall behavior for the neighboring fibers is very similar to that displayed in Fig. 6.

Figure 9 shows σ_θ/σ_0 along the matrix side of the interphase of the dissimilar fiber and $\bar{U}$ in the interphase for $\bar{k} = 10$ and $\bar{k} = 1$, for various interphase crack lengths $\bar{c}$. The results show that for $\bar{k} = 10$ the positive maximum hoop stress occurs at the crack tip and increases as c increases. On the other hand for $\bar{k} = 1$ the positive maximum hoop stress occurs near $\theta = 75°$ for $\bar{c} < 18$. Results not displayed here show that for both $\bar{k} = 1$ and $\bar{k} = 10$ the stresses σ_θ along the interphases of the neighboring fibers 1 and 2 increase locally as $\bar{c}$ increases, but there is little difference between $\bar{k} = 1$ and $\bar{k} = 10$.

A stability condition is needed when interphase cracks are present. The strain energy criterion was introduced in the papers by Achenbach and Zhu (1989, 1990) to investigate the proclivity of an interphase crack to propagate. Figure 9 shows that $\bar{U}$ plotted versus θ shows maximums at the tips of the interphase cracks of the dissimilar fiber. For $\bar{k} = 1$, the

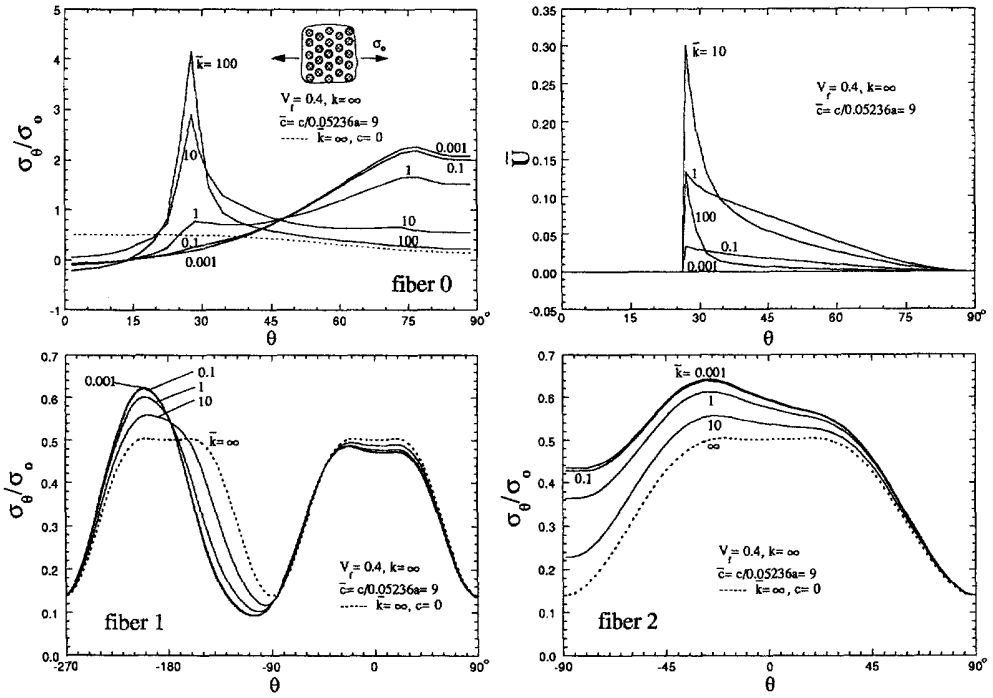

Fig. 8. σ_θ/σ_0 at the matrix sides of the interphases of the dissimilar fiber 0 and the neighboring fibers 1 and 2, and $\bar{U}$ in the interphase of fiber 0, for various $\bar{k}$ with $k = \infty$ and $V_f = 0.4$, and $\bar{c} = 9$, for uniaxial tension in the x direction.

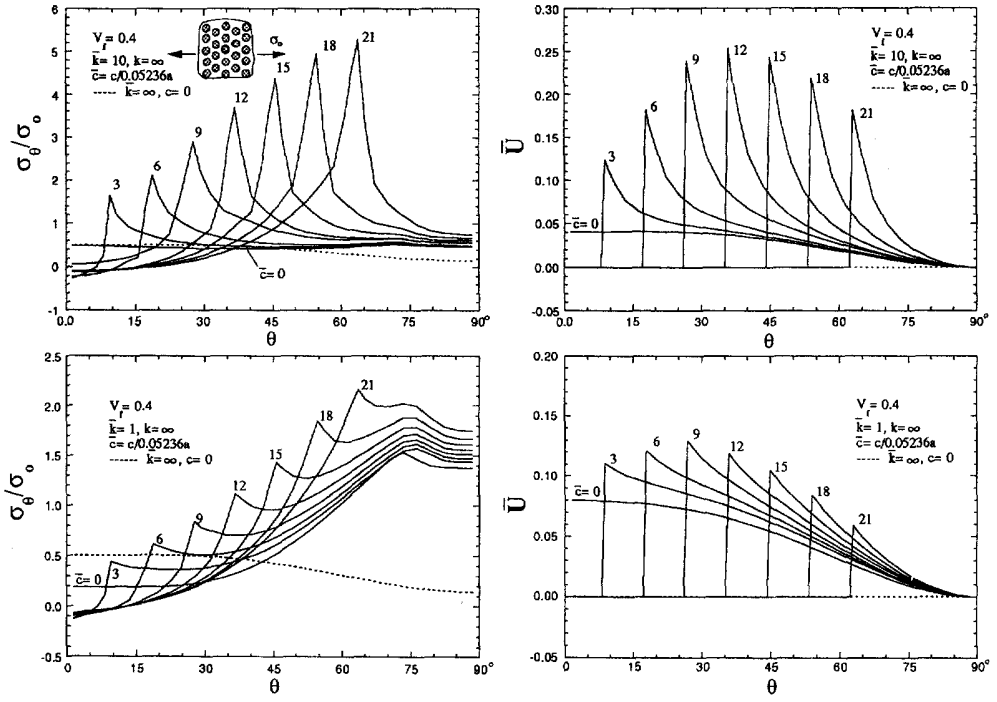

Fig. 9. σ_θ/σ_0 at the matrix side of the interphase and $\bar{U}$ in the interphase of the dissimilar fiber 0, for various $\bar{c}$ with $k = \infty$, $V_f = 0.4$ and $\bar{k} = 10$ and $\bar{k} = 1$, for uniaxial tension in the x direction.

maximum values first increase and then decrease as $\bar{c}$ increases. They become in fact smaller than for $\bar{c} = 0$, and hence the interface flaw will be arrested for that case.

CONCLUDING COMMENTS

A fiber whose interphase has a lower stiffness than the surrounding fibers, or whose interphase contains cracks, gives rise to higher fields of stress and deformation in its immediate vicinity. For the case of transverse loading, a numerical method based on the solution of boundary integral equations by the boundary element method has been developed to obtain the stresses at the matrix side of the interphases and the deformation energy density in the interphases, for the dissimilar fiber and its nearest neighbors. The example of a hexagonal array fiber composite has been discussed in some detail, and particular attention has been devoted to the hoop stresses and the deformation energy densities since critical values of these quantities may be associated with radial matrix cracking and interphase cracking, respectively.

Acknowledgement—This work was carried out in the course of research sponsored by the Air Force Office of Scientific Research (AFOSR), under the direction of Dr Walter F. Jones.

REFERENCES

Achenbach, J. D. and Choi, H. S. (1991). Matrix cracking and interphase failure in fiber composites. In *Local Mechanics Concepts for Composite Material Systems* (Edited by J. N. Reddy and K. L. Reifsnider), pp. 149–163. IUTAM Symposium Blacksburg, VA, Springer–Verlag.

Achenbach, J. D. and Zhu, H. (1989). Effect of interfacial zone on mechanical behavior and failure of fiber-reinforced composites. *J. Mech. Phys. Solids* **37,** 381–393.

Achenbach, J. D. and Zhu, H. (1990). Effect of interphases on micro- and macro-mechanical behavior of hexagonal array fiber composites. *J. Appl. Mech.* **57,** 956–963.

Benveniste, Y. (1985) The effective mechanical behavior of composite materials with imperfect contact between the constituents. *Mech. Mater.* **4,** 197–208.

Gosz, M., Moran, B. and Achenbach, J. D. (1992). Load-dependent constitutive response of fiber composites with compliant interphases. *J. Mech. Phys. Solids* **40,** 1789–1803.

Hashin, Z. (1990). Thermoelastic properties of fiber composites with imperfect interface. *Mech. Mater.* **8,** 333–348.

Hashin, Z. (1991). Thermoelastic properties of particulate composites with imperfect interface. *J. Mech. Phys. Solids* **39,** 745–762.

Hashin, Z. (1992). Extremum principles for elastic heterogeneous media with imperfect interfaces and their application to bounding of effective moduli. *J. Mech. Phys. Solids* **40,** 767–780.

Jasiuk, I., Chen, J. and Thorpe, M. F. (1992). Elastic moduli of composites with rigid sliding inclusions. *J. Mech. Phys. Solids* **40,** 373–391.

Steif, P. and Hoysan, S. F. (1987). An energy method for calculating the stiffness of aligned short-fiber composites. *Mech. Mater.* **6,** 197–210

Takahashi, K. and Chou, T. W. (1988). Transverse elastic moduli of unidirectional fiber composites with interfacial debonding. *Metall. Trans. A,* **19A,** 129–135.

Williams, M. L. (1959). The stresses around a fault or crack in dissimilar media. *Bull. Seismol. Soc. Am.* **49,** 199–204.

Zhu, H. and Achenbach, J. D. (1991). Effect of fiber-matrix interphase defects on microlevel stress states at neighboring fibers. *J. Compos. Mater.* **25,** 224–238.

APPENDIX: FIRST QUADRANT FUNDAMENTAL SOLUTIONS

The components of the two-dimensional first quadrant fundamental displacement solutions may be written as

$$U_{11}^{Q}(x,\xi) = U_{11}(x,\xi) - U_{11}(x,-\bar{\xi}) - U_{11}(x,-\xi) + U_{11}(x,\bar{\xi})$$

$$= K\left[(3-4\nu)\ln\frac{R_2R_3}{RR_4} + \left(\frac{\partial R}{\partial x_1}\right)_2 - \left(\frac{\partial R_2}{\partial x_1}\right)^2 - \left(\frac{\partial R_3}{\partial x_1}\right)^2 + \left(\frac{\partial R_4}{\partial x_1}\right)^2\right] \tag{A1}$$

where $K = 1/[8\pi\mu(1-\nu)]$. Also

$$U^{Q}_{12}(\boldsymbol{x},\boldsymbol{\xi}) = U_{12}(\boldsymbol{x},\boldsymbol{\xi}) - U_{12}(\boldsymbol{x},-\bar{\boldsymbol{\xi}}) - U_{12}(\boldsymbol{x},-\boldsymbol{\xi}) + U_{12}(\boldsymbol{x},\bar{\boldsymbol{\xi}}) = K\left[\frac{\partial R}{\partial x_1}\frac{\partial R}{\partial x_2} - \frac{\partial R_2}{\partial x_1}\frac{\partial R_2}{\partial x_2} - \frac{\partial R_3}{\partial x_1}\frac{\partial R_3}{\partial x_2} + \frac{\partial R_4}{\partial x_1}\frac{\partial R_4}{\partial x_2}\right] \tag{A2}$$

$$U^{Q}_{21}(\boldsymbol{x},\boldsymbol{\xi}) = U_{21}(\boldsymbol{x},\boldsymbol{\xi}) + U_{21}(\boldsymbol{x},-\bar{\boldsymbol{\xi}}) - U_{21}(\boldsymbol{x},-\boldsymbol{\xi}) - U_{21}(\boldsymbol{x},\bar{\boldsymbol{\xi}}) = K\left[\frac{\partial R}{\partial x_1}\frac{\partial R}{\partial x_2} + \frac{\partial R_2}{\partial x_1}\frac{\partial R_2}{\partial x_2} - \frac{\partial R_3}{\partial x_1}\frac{\partial R_3}{\partial x_2} - \frac{\partial R_4}{\partial x_1}\frac{\partial R_4}{\partial x_2}\right] \tag{A3}$$

and

$$U^{Q}_{22}(\boldsymbol{x},\boldsymbol{\xi}) = U_{22}(\boldsymbol{x},\boldsymbol{\xi}) + U_{22}(\boldsymbol{x},-\bar{\boldsymbol{\xi}}) - U_{22}(\boldsymbol{x},-\boldsymbol{\xi}) - U_{22}(\boldsymbol{x},\bar{\boldsymbol{\xi}})$$
$$= K\left[(3-4\nu)\ln\frac{R_3R_4}{RR_2} + \left(\frac{\partial R}{\partial x_2}\right)^2 + \left(\frac{\partial R_2}{\partial x_2}\right)^2 - \left(\frac{\partial R_3}{\partial x_2}\right)^2 - \left(\frac{\partial R_4}{\partial x_2}\right)^2\right]. \tag{A4}$$

Here, as shown in Fig. 2, R_2, R_3 and R_4 are the distances between the load point in the first quadrant and the image points in the second, third and fourth quadrants, respectively. Also, R is the distance between load point, $\boldsymbol{\xi}$, and the field point, $\boldsymbol{x}$. Thus,

$$R = |\boldsymbol{x}-\boldsymbol{\xi}|,\ R_2 = |\boldsymbol{x}+\bar{\boldsymbol{\xi}}|,\ R_3 = |\boldsymbol{x}+\boldsymbol{\xi}| \quad \text{and} \quad R_4 = |\boldsymbol{x}-\bar{\boldsymbol{\xi}}|. \tag{A5}$$

The first quadrant traction solutions may be expressed as

$$\begin{aligned} T^{Q}_{11}(\boldsymbol{x},\boldsymbol{\xi}) &= T_{11}(\boldsymbol{x},\boldsymbol{\xi}) - T_{11}(\boldsymbol{x},-\bar{\boldsymbol{\xi}}) - T_{11}(\boldsymbol{x},-\boldsymbol{\xi}) + T_{11}(\boldsymbol{x},\bar{\boldsymbol{\xi}}) \\ &= \frac{C}{R}\frac{\partial R}{\partial n}\left[(1-2\nu)+2\left(\frac{\partial R}{\partial x_1}\right)^2\right] - \frac{C}{R_2}\frac{\partial R_2}{\partial n}\left[(1-2\nu)+2\left(\frac{\partial R_2}{\partial x_1}\right)^2\right] \\ &- \frac{C}{R_3}\frac{\partial R_3}{\partial n}\left[(1-2\nu)+2\left(\frac{\partial R_3}{\partial x_1}\right)^2\right] + \frac{C}{R_4}\frac{\partial R_4}{\partial n}\left[(1-2\nu)+2\left(\frac{\partial R_4}{\partial x_1}\right)^2\right] \end{aligned} \tag{A6}$$

where $C = -2\mu K$. Also

$$\begin{aligned} T^{Q}_{12}(\boldsymbol{x},\boldsymbol{\xi}) &= T_{12}(\boldsymbol{x},\boldsymbol{\xi}) - T_{12}(\boldsymbol{x},-\bar{\boldsymbol{\xi}}) - T_{12}(\boldsymbol{x},-\boldsymbol{\xi}) + T_{12}(\boldsymbol{x},\bar{\boldsymbol{\xi}}) \\ &= \frac{C}{R}\left[2\frac{\partial R}{\partial n}\frac{\partial R}{\partial x_1}\frac{\partial R}{\partial x_2} + (1-2\nu)\left(n_1\frac{\partial R}{\partial x_2} - n_2\frac{\partial R}{\partial x_1}\right)\right] \\ &- \frac{C}{R_2}\left[2\frac{\partial R_2}{\partial n}\frac{\partial R_2}{\partial x_1}\frac{\partial R_2}{\partial x_2} + (1-2\nu)\left(n_1\frac{\partial R_2}{\partial x_2} - n_2\frac{\partial R_2}{\partial x_1}\right)\right] \\ &- \frac{C}{R_3}\left[2\frac{\partial R_3}{\partial n}\frac{\partial R_3}{\partial x_1}\frac{\partial R_3}{\partial x_2} + (1-2\nu)\left(n_1\frac{\partial R_3}{\partial x_2} - n_2\frac{\partial R_3}{\partial x_1}\right)\right] \\ &+ \frac{C}{R_4}\left[2\frac{\partial R_4}{\partial n}\frac{\partial R_4}{\partial x_1}\frac{\partial R_4}{\partial x_2} + (1-2\nu)\left(n_1\frac{\partial R_4}{\partial x_2} - n_2\frac{\partial R_4}{\partial x_1}\right)\right]. \end{aligned} \tag{A7}$$

$$\begin{aligned} T^{Q}_{21}(\boldsymbol{x},\boldsymbol{\xi}) &= T_{21}(\boldsymbol{x},\boldsymbol{\xi}) + T_{21}(\boldsymbol{x},-\bar{\boldsymbol{\xi}}) - T_{21}(\boldsymbol{x},-\boldsymbol{\xi}) - T_{21}(\boldsymbol{x},\bar{\boldsymbol{\xi}}) \\ &= \frac{C}{R}\left[2\frac{\partial R}{\partial n}\frac{\partial R}{\partial x_1}\frac{\partial R}{\partial x_2} - (1-2\nu)\left(n_1\frac{\partial R}{\partial x_2} - n_2\frac{\partial R}{\partial x_1}\right)\right] \\ &+ \frac{C}{R_2}\left[2\frac{\partial R_2}{\partial n}\frac{\partial R_2}{\partial x_1}\frac{\partial R_2}{\partial x_2} - (1-2\nu)\left(n_1\frac{\partial R_2}{\partial x_2} - n_2\frac{\partial R_2}{\partial x_1}\right)\right] \\ &- \frac{C}{R_3}\left[2\frac{\partial R_3}{\partial n}\frac{\partial R_3}{\partial x_1}\frac{\partial R_3}{\partial x_2} - (1-2\nu)\left(n_1\frac{\partial R_3}{\partial x_2} - n_2\frac{\partial R_3}{\partial x_1}\right)\right] \\ &- \frac{C}{R_4}\left[2\frac{\partial R_4}{\partial n}\frac{\partial R_4}{\partial x_1}\frac{\partial R_4}{\partial x_2} - (1-2\nu)\left(n_1\frac{\partial R_4}{\partial x_2} - n_2\frac{\partial R_4}{\partial x_1}\right)\right] \end{aligned} \tag{A8}$$

and

$$T_{22}^{Q}(\boldsymbol{x},\boldsymbol{\xi}) = T_{22}(\boldsymbol{x},\boldsymbol{\xi}) + T_{22}(\boldsymbol{x},-\bar{\boldsymbol{\xi}}) - T_{22}(\boldsymbol{x},-\boldsymbol{\xi}) - T_{22}(\boldsymbol{x},\bar{\boldsymbol{\xi}})$$
$$= \frac{C}{R}\frac{\partial R}{\partial n}\left[(1-2\nu)+2\left(\frac{\partial R}{\partial x_2}\right)^2\right] + \frac{C}{R_2}\frac{\partial R_2}{\partial n}\left[(1-2\nu)+2\left(\frac{\partial R_2}{\partial x_2}\right)^2\right] \tag{A9}$$
$$-\frac{C}{R_3}\frac{\partial R_3}{\partial n}\left[(1-2\nu)+2\left(\frac{\partial R_3}{\partial x_2}\right)^2\right] - \frac{C}{R_4}\frac{\partial R_4}{\partial n}\left[(1-2\nu)+2\left(\frac{\partial R_4}{\partial x_2}\right)^2\right].$$

It can be verified that the first quadrant fundamental solutions satisfy the following boundary conditions on axes of symmetry:

$$U_{i1}(\boldsymbol{x},\boldsymbol{\xi}) = T_{i2}(\boldsymbol{x},\boldsymbol{\xi}) = 0, \quad \boldsymbol{x}\in(x=0, y\geqslant 0) \tag{A10}$$

$$U_{i2}(\boldsymbol{x},\boldsymbol{\xi}) = T_{i1}(\boldsymbol{x},\boldsymbol{\xi}) = 0, \quad \boldsymbol{x}\in(x\geqslant 0, y=0). \tag{A11}$$

Here the subscript i denotes the load direction and takes a value of 1 or 2, while the second subscript indicates the displacement or traction direction.